Int. J. Solids Structures Vol. 27, No. 1, pp. 89–103, 1991
Printed in Great Britain.

0020–7683/91 $3.00 + .00

DYNAMIC PLASTIC BUCKLING OF COPPER CYLINDRICAL SHELLS

A. L. FLORENCE, P. R. GEFKEN and S. W. KIRKPATRICK
Poulter Laboratory, Physical Science Division, SRI International, 333 Ravenswood Avenue, Menlo Park, CA 94025, U.S.A.

(*Received* 20 *May* 1989; *in revised form* 9 *November* 1989)

Abstract—The dynamic plastic buckling of annealed OFHC copper cylindrical shells is treated by experiment, finite element code calculation, and analysis. Initial velocity imperfections of the impulsive loading were obtained from sheet explosive thickness measurements. The Johnson–Cook relation was adopted for the copper. A comparison of the final profiles, their modal content, and amplification functions showed good agreement among experimental, code and analytical results

INTRODUCTION

Our research on the explosively-formed penetrator (EFP), a conventional weapon, has involved the application of the finite element code DYNA3D (Hallquist, 1988). EFPs consist of a shallow metallic dish in front of encased explosive. As shown in Fig. 1 when the explosive is detonated, the dish is projected and deformed into a projectile of tubular shape. Large convergent plastic flow occurs that is almost axisymmetric but accompanied by dynamic plastic buckling. The late stage of formation is similar to that of a cylindrical shell responding to a radially inward impulse.

In order to acquire confidence in the finite element solution, we applied the code directly to the less complex case of a cylindrical shell subjected to a radially inward impulse. This case was also solved by classical analysis (Lindberg and Florence, 1987) to allow a quantitative comparison of the final shapes and the spectral distributions of the amplitudes of the modes forming the final shape. The same initial imperfections and approximately the same dynamic constitutive equations were used in the code calculations and the analysis.

To evaluate the theoretical descriptions of the dynamic plastic buckling, we performed experiments on cylindrical shells of annealed OFHC copper in which the shells were subjected to a uniform impulse from sheet explosive wrapped around the shells. Initial velocity imperfections were obtained from thickness measurements of the explosive sheet. The final profiles of the shells were measured and the modal distributions obtained for comparisons with the corresponding results from the code and analysis. The main subject for evaluation was the applicability to our shell problem, of the constitutive equations in the Johnson–Cook (1983) form, based on the dynamic tensile tests of Rajendran and Bless (1985). Five shells were impulsively loaded at increasing intensity. Comparisons are presented for the shell subjected to the largest impulse, which resulted in a final average

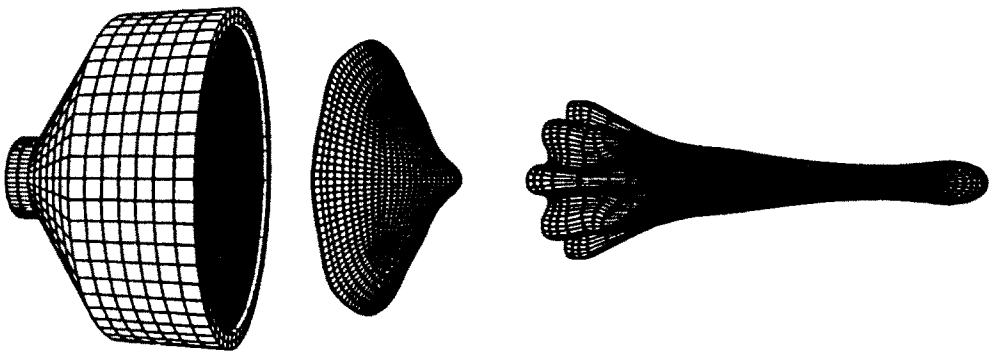

Fig. 1. Simulation of penetrator formation.

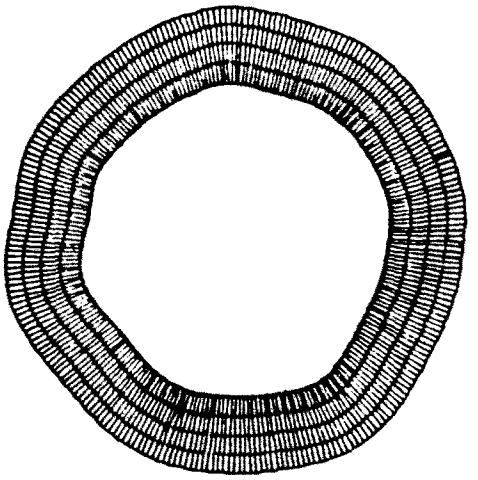

Fig. 2. Calculated final deformation with dynamic plastic buckles (radial displacements shown with ×3 magnification).

hoop engineering strain of 18.3%. For a description of dynamic plastic buckling with average hoop strains up to this magnitude, we found that the radius decrease and thickness increase had to be included in the analysis.

The amplitude of the dynamic plastic buckles in the copper cylinder subjected to the largest impulse intensity, was approximately 0.5–1.0% of the initial radius (0.018–0.035 mm). These buckles are small in amplitude yet can be detected manually in the post-test inspection. Figure 2 shows a buckled cylinder profile from a finite element calculation corresponding to this experiment. The displacements in the figure have been amplified by a factor of three to make the buckles more apparent. These buckles in the copper cylinder are considerably smaller than those shown on the explosively formed penetrator in Fig. 1. However, the ability to accurately model the initial buckle growth in the copper cylinders is a necessary condition for modeling the large amplitude buckles growth in the copper cylinders, which is a necessary condition for modeling the large amplitude buckles in the penetrator. A comparison of the finite element solution with the experiment and classical analysis for the buckling of the copper cylinder allows us to validate that at least the initiation of the plastic buckling in the penetrator is accurately modeled in the numerical simulation.

The presentation starts with a brief description of the experiments, followed by a description of the finite element simulations, an outline of the analysis and concludes with a comparison of the results. The main conclusion of the work is that the finite element code, DYNA3D, produced final shell profiles and amplification spectra in very good agreement with analytical results and by comparison with experimental results, gave a very good description of the dynamic plastic buckling; hence, the Johnson–Cook dynamic constitutive equation was applicable to the problem. Although the application of the code is for cases with larger plastic deformations, as illustrated in Fig. 1, the simpler evaluation case of cylindrical shells provides some confidence in the code performance, especially because of the excellent treatment of an instability phenomena involving growth that is temporally exponential.

EXPERIMENTS

The experimental arrangement is shown in Fig. 3. The annealed OFHC copper cylinders were 10 cm (3.9 in.) long, 7.37 cm (2.9 in.) in outside diameter, and had a uniform wall thickness of 3.81 mm (0.15 in.). With respect to the midsurface radius of 3.493 cm, the initial radius-to-thickness ratio of each shell was 9.17. The cylinders were enclosed in

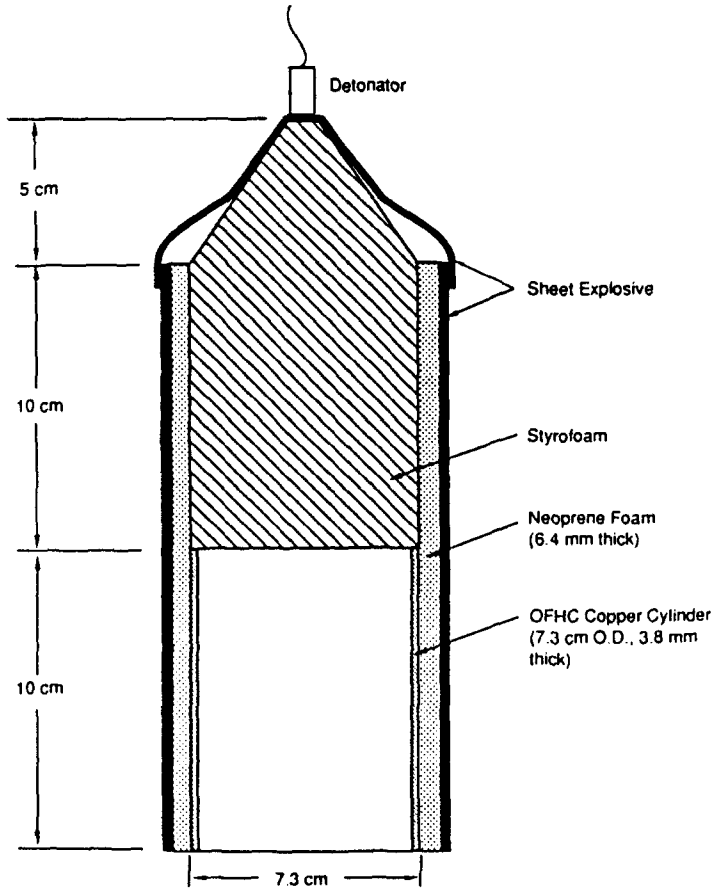

Fig. 3. Experimental arrangement for imploding copper cylinders.

an attenuator of 6.4 mm thick (0.25 in.) neoprene foam around which was wrapped a layer of sheet explosive (EL506D). The foam prevents spall and reduces the initial shock wave magnitude. As shown in Fig. 3, the neoprene foam and sheet explosive were extended beyond the top of the cylinder by 10 cm and then tailored to converge to a detonator on axis. The detonation front sweeps over the cylinder at a speed of 7 km s^{-1}, which is supersonic relative to the elastic wave speed of copper (4 km s^{-1}). Florence (1965) has shown that this supersonic loading is equivalent to a uniform impulse applied simultaneously to the cylinder surface.

Perturbations in the impulse come from variations in thickness of the sheet explosive. The thickness sampling was taken at 64 equidistant points on a line that becomes circumferential when the explosive is wrapped around the attenuator. These data were then represented in spectral form by determining their Fourier coefficients as shown in the Appendix. The impulse per unit area, I, was taken from the work of Romander (1987). For our configuration, the impulse calibration constant I_0 (impulse per unit area per unit explosive thickness) is $I_0 = 266{,}000$ dyne-sec cm^{-3}. Initial geometric imperfections were not considered because measurements indicated that precise machining of the cylindrical shells was achieved.

The post-test profiles of the five cylindrical shells were measured by rotating each cylinder about its axis in a specifically designed apparatus resembling a lathe having a fixed, radially oriented, linear variable differential transformer (LVDT). The LVDT was part of the circuit containing an amplifier and a digital oscilloscope. As in the case of the explosive thickness imperfections, the final shapes were represented in spectral form by determining their Fourier coefficients as shown in the Appendix: 2048 data points were used.

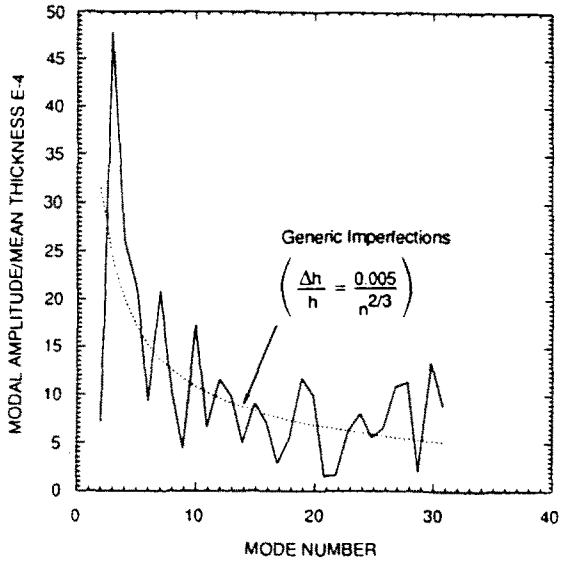

Fig. 4. Spectral distribution of explosive thickness in experiment.

Only the results for the cylindrical shell that received the largest impulse (38,900 dyne-sec cm^{-2}) are presented for comparison with the code and analytic results because this case had the largest strains (max ε_θ = 18.3%) and much more perceptible dynamic plastic buckling. The other shells were subjected to impulses ranging from 17,000 to 37,700 dyne-sec cm^{-2} resulting in final hoop strains ranging from 6.6 to 17.0%. Partial comparisons indicated good agreement throughout.

Figure 4 shows the spectral distribution of the explosive thickness obtained by applying the procedure described in the Appendix. Also shown is a smooth curve through the experimental spectrum to represent a generic spectrum. Kirkpatrick and Holmes (1989) have shown that such spectra for initial displacement and velocity imperfections lead to a correct description of buckling. If many similar experiments are involved in an investigation, only representative initial measurements will be required. These generic imperfections were used in the DYNA3D calculations and the analysis, as well as the actual imperfections.

FINITE ELEMENT SIMULATIONS

The dynamic buckling of the explosively-loaded copper tubes was simulated using DYNA3D (Hallquist, 1988). DYNA3D is an explicit three-dimensional finite element code (an explicit finite element code allows the solution to be advanced without the necessity of global equation solving) for analyzing the large deformation dynamic response of solids and structures. The equations of motion are integrated in time using the central difference method. Spatial discretization was achieved with eight-node solid hexahedron elements with one point integration and hourglass viscosity to control zero energy modes. The Johnson–Cook constitutive equation was used as described in the following section.

The mesh for the rings consisted of 256 elements around the circumference of the ring, four elements through the thickness of the ring, and one element along the length. The nodes were constrained in the axial direction to provide a plane strain condition. The impulsive radial load was modeled as an initial inward velocity. Imperfections in the load were included as a Fourier series perturbation to the uniform initial velocity as described in the Appendix.

CONSTITUTIVE EQUATIONS

An appropriate constitute equation for large plastic deformation of annealed OFHC copper is the Johnson–Cook relation

$$\sigma = (A + B\varepsilon^{\gamma})(1 + C\ln\dot{\varepsilon}^*)(1 - T^{*m}), \tag{1}$$

where

σ = equivalent flow stress
ε = equivalent plastic strain
$\dot{\varepsilon}^* = \dot{\varepsilon}/\dot{\varepsilon}_0$ = dimensionless strain rate ($\dot{\varepsilon}_0 = 1\ \mathrm{s}^{-1}$)
$T^* = (T - T_{\mathrm{room}})/(T_{\mathrm{melt}} - T_{\mathrm{room}})$ = homologous temperature.

We found that the constants A, B, C and γ that fit the Rajendran and Bless (1985) dynamic tensile test data for strains up to 20% at room temperature are

$A = 0.9$ kbar (90 MPa)
$B = 6.8$ kbar (680 MPa)
$C = 0.044$
$\gamma = 0.9$.

Examination of eqn (1) revealed that two approximations concerning temperature and strain rate could be introduced into the analysis. For strains of less than 20% the temperature rise in copper is such that $T^{*m} \ll 1$ (the constitutive equation value of m is about 2). Secondly, the strain rate term

$$R(\dot{\varepsilon}^*) = 1 + C\ln\dot{\varepsilon}^* \approx 1.32, \tag{2}$$

over a wide range of strain rates. In our cylinder, the initial strain rate is about 3200 s^{-1} and the stress-strain curves for various strain rates are within 10% of each other down to about 320 s^{-1}. At this rate, about 99% of the initial kinetic energy has been absorbed.

An approximation introduced into the analysis and the finite element simulation is the assumption that the central region of the shell is responding in plane strain. In the analysis, this approximation for purely radial motion (unperturbed motion) along with zero radial stress (shell theory) reduce eqn (1) to

$$\sigma_\theta = \sigma_0 + k\varepsilon_\theta^{\gamma}, \tag{3}$$

where

$$\sigma_0 = \frac{2}{\sqrt{3}} AR, \quad k = \frac{2}{\sqrt{3}} B\left(\frac{2}{\sqrt{3}}\right)^{\gamma} R, \quad R = 1.32. \tag{4}$$

The initial kinetic energy determined by using the impulse calibration value equaled the plastic work done using the constitutive equation given by (3) and (4) with the constants A, B and γ listed above. For this energy balance calculation, the thickness and radius changes had to be included for good agreement.

UNPERTURBED MOTION

Let the uniform inward displacement be $w_0(t)$, where t denotes time, the initial radius and thickness be a_0 and h_0, and the current radius and thickness be $a(t)$ and $h(t)$. Then,

$$w_0(t) = a_0 - a(t) \quad h(t) = a_0 h_0 / a(t) \tag{5}$$

and the circumferential thrust is

$$N = (\sigma_0 + k\varepsilon_\theta^{\gamma})h. \tag{6}$$

Substitution of (6) in the equation of motion

$$N = -\rho h a \ddot{w}_0$$

gives

$$\ddot{w}_0 + \frac{1}{\rho a}\left\{\sigma_0 + k\left(\frac{w_0}{a_0}\right)^{\gamma}\right\} = 0, \tag{7}$$

where ρ is the density of the shell material. In (7), we have made the approximation $\varepsilon_\theta \approx w_0/a_0$.

If we introduce the dimensionless quantities

$$u_0 = w_0/a_0, \quad \tau = ct/a_0, \quad c^2 = k/\rho, \quad \alpha = \sigma_0/k, \quad v = V/c, \tag{8}$$

where $V = I/\rho h_0$ is the initial velocity, eqn (7) becomes

$$(1-u_0)\ddot{u}_0 + u_0^{\gamma} = -\alpha. \tag{9}$$

An approximate first integral of (9) is

$$\dot{u}_0^2 = v^2 - 2\{\alpha + u_0^{\gamma}/(1+\gamma)\}u_0 - \{\alpha + 2u_0^{\gamma}/(2+\gamma)\}u_0^2. \tag{10}$$

The second integral is

$$\tau = \int_0^{u_0(\tau)} \frac{\mathrm{d}u_0}{[v^2 - 2\{\alpha + u_0^{\gamma}/(1+\gamma)\}u_0 - \{\alpha + 2u_0^{\gamma}/(2+\gamma)\}u_0^2]^{1/2}}. \tag{11}$$

This integral is used in the numerical solution of the analytic formulation but not in the approximate solution. Let $\bar{u}_0 = u_0(\bar{\tau})$ be the final engineering strain. Then, eqn (10) with $\dot{u}_0(\bar{\tau}) = 0$ gives the dimensionless energy equation

$$\{\alpha + \bar{u}_0^{\gamma}/(1+\gamma)\}\bar{u}_0 + \{\alpha/2 + \bar{u}_0^{\gamma}/(2+\gamma)\}\bar{u}_0^2 = v^2/2. \tag{12}$$

PERTURBED MOTION

Figure 5 shows a cylindrical shell element being subjected to a thrust N, a shear Q, and a bending moment M. The inward, unperturbed displacement is $w_0(t)$, and the perturbed

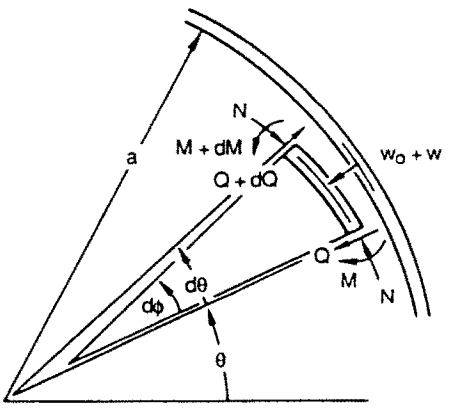

Fig. 5. Cylindrical shell element.

displacement is $w(\theta, t)$, giving a total inward displacement of $w_0(t)+w(\theta, t)$. The equations of rotary and translatory motion are

$$Q = \frac{1}{a}\cdot\frac{\partial M}{\partial \theta}, \quad \frac{1}{a}\frac{\partial Q}{\partial \theta} + N\cdot\frac{1}{a}\frac{\partial \phi}{\partial \theta} = -\rho h(w_0+w)'' \tag{13}$$

where

$$\frac{1}{a}\frac{\partial \phi}{\partial \theta} = \frac{1}{a_0} + \frac{1}{a^2}(w_0+w) + \frac{1}{a^2}\frac{\partial^2 w}{\partial \theta^2} = \frac{1}{a_0} + \kappa \tag{14}$$

is the curvature. In (14), κ represents the curvature and is given by

$$\kappa = \frac{1}{a} + \frac{1}{a^2}(w+w'') - \frac{1}{a_0}. \tag{15}$$

Elimination of Q and ϕ from (13) and (14) and use of the unperturbed equation of motion leads to

$$M'' + N(w+w'') + a^2\rho h\ddot{w} = 0, \tag{16}$$

where primes denote differentiation with respect to θ.

The bending moment is

$$M = -\int_{h/2}^{h/2} \sigma_0(z) z\, dz = \frac{kh^3}{12}\gamma\kappa\dot{\varepsilon}_0^{1-\gamma}, \tag{17}$$

in which $\dot{\varepsilon}_0$ is the hoop strain rate at the midsurface of the shell.

Substitution of the thrust N and moment M, given by (6) and (17), in the equation of motion (16) leads to the equation governing the perturbed displacement $w(\theta, t)$. Converting this equation to dimensionless form using (8) and

$$u = w/a_0 \quad \beta = h_0^2/12a_0^2 \tag{18}$$

results in

$$\ddot{u} + (\alpha+u_0^{\gamma})(1-u_0)^{-2}(u+u'') + \beta\gamma u_0^{-(1-\gamma)}(1-u_0)^{-6}(\gamma u+u'')'' = 0, \tag{19}$$

with superscript dots and primes denoting differentiation with respect to τ and θ. In deriving (19), products of perturbation terms were neglected and binomial approximations were made.

MODAL SOLUTION

Let the dimensionless perturbed displacements $u(\theta, \tau)$ be represented in the Fourier form:

$$u(\theta, \tau) = \sum_{n=2}^{\infty} \{D_n(\tau)\cos(n\theta) + E_n(\tau)\sin(n\theta)\}, \tag{20}$$

in which D_0, D_1 and E_1 are omitted because D_0 would only contribute to the unperturbed displacement and D_1 and E_1 would describe rigid body translation. Substitute (20) in the governing eqn (19) and equate to zero the coefficients of cos $(n\theta)$ and sin $(n\theta)$. Then we obtain two sets of ordinary differential equations for the coefficients D_n and E_n. These sets

are

$$\ddot{D}_n - f_n(\tau)D_n = 0, \quad \ddot{E}_n - f_n(\tau)E_n = 0, \quad n = 2,3,\ldots \tag{21}$$

where

$$f_n(\tau) = (1-u_0)^{-2}\{(\alpha+u_0^\gamma)(n^2-1) - \beta\gamma n^2(n^2-\gamma)(1-u_0)^{-4}u_0^{-(1-\gamma)}\}. \tag{22}$$

The form of the function $f_n(\tau)$ is shown in Fig. 6. Because $\gamma < 1$, the function $f_n(\tau)$ is singular and negative at the start of the motion. Substantial growth of D_n and E_n cannot occur until $f_n(\tau)$ becomes positive. If $f_n(\tilde{\tau}_n) = 0$, growth occurs only after time $\tilde{\tau}_n$, when $f_n(\tau) > 0$ $(\tilde{\tau}_n < \tau < \bar{\tau})$. This condition, according to (22), means that growth occurs only in modes with mode numbers that are less than some cut-off value $N(\tau)$ where

$$N^2(\tau) \approx (\alpha+u_0^\gamma)u_0^{1-\gamma}(1-u_0)^4/\beta\gamma, \quad \tau > \tilde{\tau}_n. \tag{23}$$

The numerical values for our cylinder ($\alpha = 0.116$, $\beta = 10^{-3}$, $\gamma = 0.9$ and $\bar{u}_0 = 0.183$) give $N(\bar{\tau}) = 12$, that is, modes defined by $n = 2, 3, \ldots, 12$ are amplified. If we estimate the preferred mode number by maximizing $f_n(\bar{\tau})$ with respect to n we obtain $\bar{n} = N/\sqrt{2}$, which for our cylinder gives $n = 8$ or 9. However, according to (22), the lower the mode number, the longer the finite amplification time, $\bar{\tau} - \tilde{\tau}_n$. Each Fourier component representing thrust and resistive moment has different relative values at each instant, given by $u_0(\tau)$ in (22), and for each mode the thrust increases monotonically and the resistive moment decreases monotonically with time increase, thereby producing modal instability.

The Fourier series representation of the dimensionless initial velocity imperfections is

$$\dot{u}(\theta,0) = v\sum_{n=2}^{\infty}\{a_n\cos(n\theta) + b_n\sin(n\theta)\}. \tag{24}$$

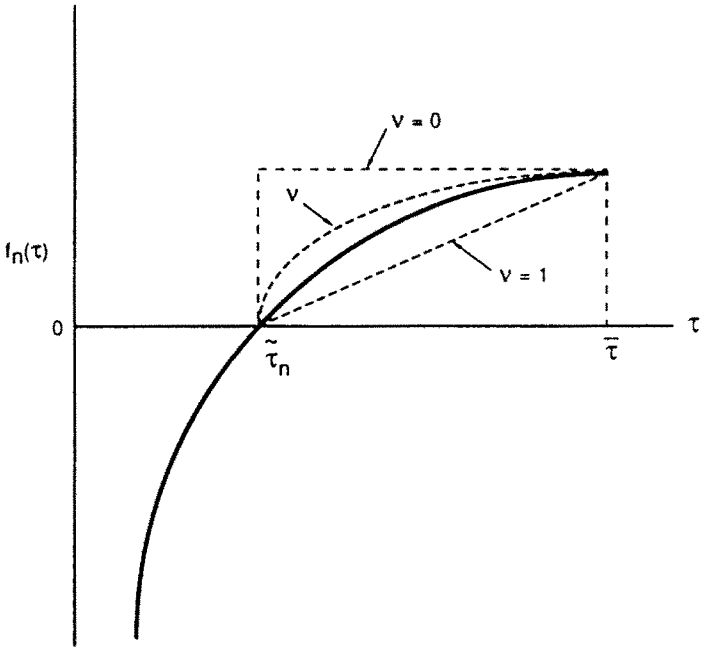

Fig. 6. Typical fundamental problem coefficient with approximations.

where $v = V/c$, V being the initial unperturbed uniform velocity. In (24), the coefficients are the same as the coefficients determined from the explosive thickness measurements, as described in the Appendix. With the assumption that the initial geometric imperfections are negligible, the initial conditions for the functions $D_n(\tau)$ and $E_n(\tau)$ are

$$D_n(0) = 0, \quad \dot{D}_n(0) = va_n, \quad E_n(0) = 0, \quad \dot{E}_n(0) = vb_n. \tag{25}$$

In terms of the set of fundamental problems.

$$\ddot{A}_n - f_n(\tau)A_n = 0, \tag{26}$$

$$A_n(0) = 0, \quad \dot{A}_n(0) = 1, \tag{27}$$

we have

$$D_n(\tau) = A_n(\tau)va_n, \quad E_n(\tau) = A_n(\tau)vb_n, \tag{28}$$

so that (20) may be written as

$$u(\theta, \tau) = v \sum_{n=2}^{\infty} A_n(\tau)\{a_n \cos(n\theta) + b_n \sin(n\theta)\} \tag{29}$$

$$= v \sum_{n=2}^{\infty} A_n(\tau)c_n \cos(n\theta + \phi_n). \tag{30}$$

By comparing the representations (24) and (29), we see that the perturbed current displacement is obtained from the initial velocity imperfections by multiplying the nth mode by the function $A_n(\tau)$. The function $A_n(\tau)$ is the amplification function. Figure 7 shows the spectral distribution of the amplification function at four times ($\frac{1}{4}\bar{\tau}$, $\frac{1}{2}\bar{\tau}$, $\frac{3}{4}\bar{\tau}$, $\bar{\tau}$) obtained by numerical solution of the fundamental problem (26) and (27). At the final time $\bar{\tau}$, the preferred mode numbers are $\bar{n} = 8$ and 9, and the maximum value of A_n is about $A_8(\bar{\tau}) = 3.9$. The profile obtained with $A_n(\bar{\tau})$ is shown in the section below where the experimental, DYNA3D code, and analytic results are compared.

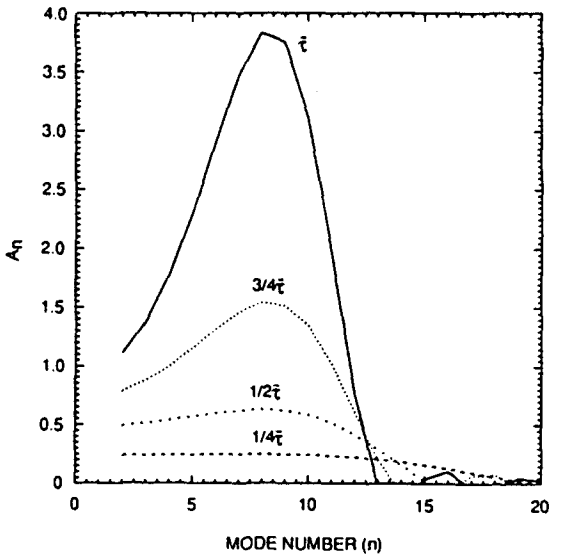

Fig. 7. Growth of amplification spectra.

APPROXIMATE SOLUTIONS

We made several approximations in our analysis to derive formulae for the preferred mode number and the amplification function. These formulae provide explicitly the dependence of the preferred mode number and the growth of the modal amplitude on the geometrical and material properties.

We outline the approximating procedure and present the results of the sequence of steps taken. The approximations are appropriate for the parameter range $0.8 < \gamma < 1.0$. For other ranges, similar approximations can readily be made. For a specific impulse or initial velocity, the energy eqn (12) determines the final hoop strain, $\bar{u}_0$. Our approximating procedure for determining $\bar{u}_0$, the hoop strain that gives $f_n = 0$, showed that for γ in the above range, we may take $\bar{u}_0 \approx 0$ except for the last mode that can be amplified. This procedure consisted of linearizing certain terms in $f_n(u_0)$, given by (22). The result, $\bar{u}_0 = u_0(\bar{\tau}_n) = 0$, allowed us to take $\bar{\tau}_n \approx 0$. It is interesting to note that if the exponent γ has smaller values, say $0.3 < \gamma < 0.7$, the values of $\bar{\tau}_n$ no longer form a cluster near the time origin.

To find a formula for the dimensionless duration of motion, we consider the unperturbed motion of a shell with linear hardening for the same final stress and strain, that is,

$$\sigma_0 = \sigma_1 + k_1 \varepsilon_0, \quad \bar{\varepsilon}_0 = \bar{u}_0, \quad \bar{\sigma}_0 = \sigma_0 + k\bar{\varepsilon}_0^{\gamma}. \tag{31}$$

Let the unperturbed strain for this case be $u_1(\tau_1)$. Then

$$(1 - u_1)\ddot{u}_1 + u_1 = -\alpha_1 \tag{32}$$

is the equation of unperturbed motion in which

$$\tau_1 = c_1 t/a_0, \quad c_1^2 = k_1/\rho, \quad \alpha_1 = \sigma_1/k_1, \quad v_1 = V/c_1. \tag{33}$$

If during integration of (32) we let $2u_1^3/3 \approx 2u_1^2\bar{u}_1/3$, we can derive the approximation for the duration of motion,

$$\bar{\tau}_1 = \frac{1}{(1+\alpha_1+2\bar{u}_0^2/3)^{1/2}}\left\{\frac{\pi}{2} - \sin^{-1}\frac{\alpha_1}{(1+\alpha_1+2\bar{u}_0^2/3)\bar{u}_0+\alpha_1}\right\}. \tag{34}$$

The values of σ_1 and k_1 and hence α_1 are found explicitly from (31) and the assumption that the plastic work is the same with linear hardening as in the Johnson–Cook case being solved (same areas under the stress–strain curves). These conditions of the same final stress, strain and plastic work give

$$\alpha_1 = \alpha + \frac{2}{2+\bar{\mu}_0}\left\{\frac{\bar{u}_0^{\gamma}}{1+\gamma} - \frac{\bar{u}_0}{2} + \left(\frac{\bar{u}_0^{\gamma}}{2+\gamma} - \frac{\bar{u}_0}{3}\right)\bar{u}_0\right\}. \tag{35}$$

We assume that the duration we require is given by $\bar{\tau} = \bar{\tau}_1$.

The final approximation is for the positive portion of $f_n(\tau)$ given by (22). A mathematically convenient form is $f_n(\tau) \approx [(\tau - \bar{\tau}_n)/(\bar{\tau} - \bar{\tau}_n)]^{\nu} f_n(\bar{\tau})$ with the exponent ν in the range $0 \leqslant \nu \leqslant 1$. This form is illustrated in Fig. 6 including the upper and lower bound values $\nu = 0$ and $\nu = 1$. Because in our case $\bar{\tau}_n \approx 0$, we may use $f_n(\tau) \approx (\tau/\bar{\tau})^{\nu} \bar{f}_n$. With this approximation, the fundamental problem (26) and (27) becomes

$$\ddot{A}_n(\xi) - \lambda_n^2 \xi^{\nu} A_n(\xi) = 0 \tag{36}$$

$$A_n(0) = 0 \quad \dot{A}_n(0) = \bar{\tau}. \tag{37}$$

where

$$\xi = \tau/\bar{\tau}\,(0 < \xi < 1) \quad \lambda_n = \bar{\tau}\bar{f}_n. \tag{38}$$

Equation (36) is the Cayley equation and its solution satisfying the initial conditions (37) may be expressed as

$$A_n(\xi) = \bar{\tau}\Gamma(1+\mu)\cdot(\mu\lambda_n)^{-\mu}\xi^{1/2}I_\mu(2\mu\lambda_n\xi^{1/2\mu}), \tag{39}$$

in which $\mu = (2+\nu)^{-1}$, Γ is the gamma function, and I_μ is the modified Bessel function of order μ.

The upper and lower bounding cases $\nu = 0$ and $\nu = 1$ of the amplification function (39) are

$$A_n(\tau) = \bar{f}_n^{-1/2}\sinh \bar{f}_n^{1/2}\tau \quad (\text{case } \nu = 0), \tag{40}$$

$$A_n(\xi) = \bar{\tau}\Gamma(4/3)\cdot(3/\lambda_n)^{1/3}\xi^{1/2}I_{1/3}(2\lambda_n\xi^{3/2}/3) \quad (\text{case } \nu = 1). \tag{41}$$

For the parametric values of our cylindrical shell problem, we can apply the asymptotic forms of (40) and (41) for the final values at $\tau = \bar{\tau}$ or $\xi = 1$. Thus, (40) and (41) simplify to

$$A_n(\bar{\tau}) = (\bar{\tau}/\lambda_n)e^{\lambda_n} \quad (\text{case } \nu = 0), \tag{42}$$

$$A_n(\bar{\tau}) = \{\bar{\tau}\Gamma(1/3)/3^{1/6}2\pi^{1/2}\lambda_n^{5/6}\}e^{2\lambda_n/3} \quad (\text{case } \nu = 1). \tag{43}$$

Figure 8 shows the spectral distributions of the amplification functions at $\tau = \bar{\tau}$ given by the forms (42) and (43). Also shown for comparison is the numerical solution which lies between the bounds. In all cases, the preferred modes numbers are $\bar{n} = 8$ and 9.

If we maximize $A_n(\bar{\tau})$ in (42) and (43) with respect to the mode number n and express the result in physical quantities, we obtain

$$\bar{n} = N/\sqrt{2} = (6\bar{\sigma}_0/\bar{E}_h)^{1/2}(\bar{a}/\bar{h}), \tag{44}$$

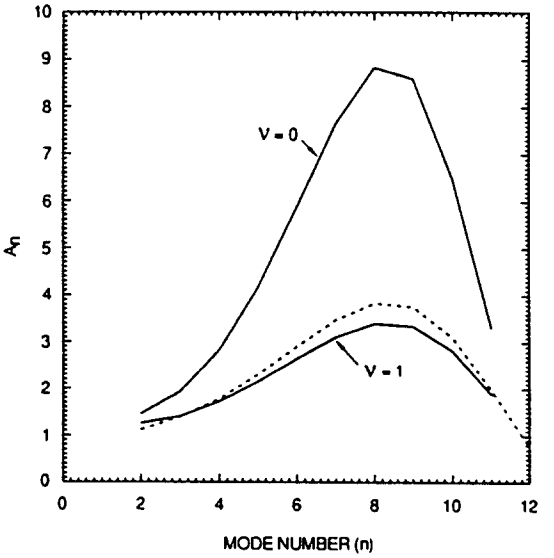

Fig. 8. Bounding amplification function spectra.

in which $\bar{E}_h$ is the slope of the stress–strain curve at the final stress $\bar{\sigma}_\theta$ and strain $\bar{\varepsilon}_\theta = \bar{u}_0$. Also, $\bar{a}$ and $\bar{h}$ are the final values of the radius and thickness: $\bar{a} = a_0(1-\bar{u}_0)$ and $\bar{h} = h_0(1-u_0)$.

COMPARISON OF RESULTS

Comparisons were made of the final profiles, their modal content, and the amplification functions obtained from experiment, DYNA3D finite element calculations, and numerical solution of the analysis. Results for measured and generic velocity imperfections are presented.

Table 1 lists the maximum displacement amplitudes, the preferred mode numbers, and the maximum modal amplitudes. In symbolic form, these are max $|w|$, $\bar{n}$, and max $|w/n|a$ = max $|u_n|$. The agreement is good, especially between DYNA3D and analysis results in which the dynamic properties are almost the same. Agreement with the experimental result shows

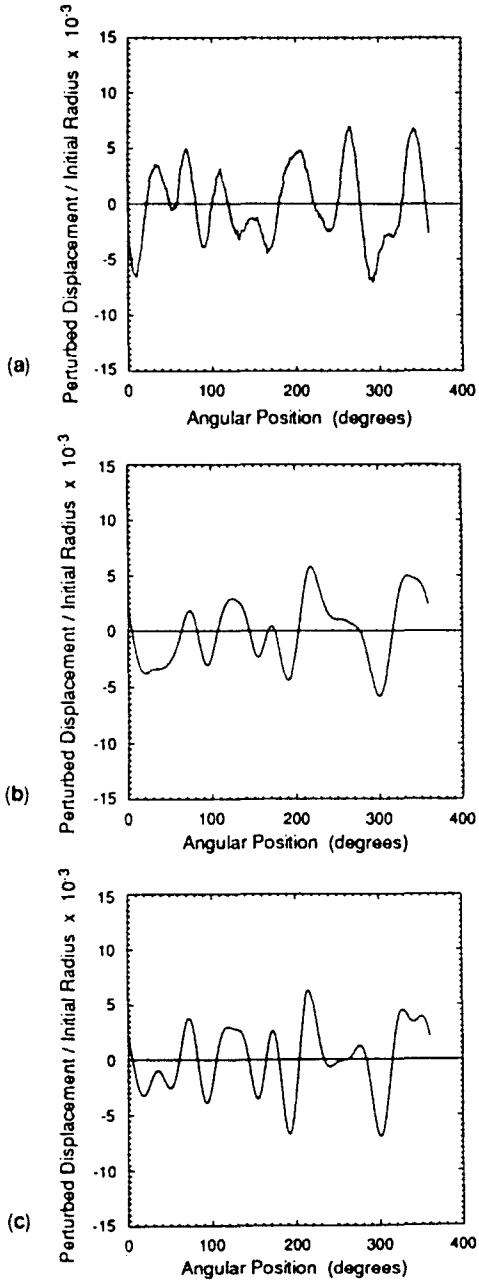

Fig. 9. Perturbed displacement profiles: (a) experiment; (b) DYNA3D; (c) analysis.

that generalization of the material properties from dynamic tensile tests is reasonable. The same conclusions are drawn from the profiles shown in Fig. 9. Small departures of the experimental profile are attributed to the influence of initial velocity imperfections, that is, explosive thickness measurements varying on either side of the axial station that was treated by DYNA3D and analysis. Figure 10 shows that for both actual and generic velocity imperfections, the modal content is similar between DYNA3D and analysis but weighed toward the lower modes in the code results. The modal content of the experimental profile lies within the theoretical distributions but with slightly higher peaks.

Figure 11 shows that DYNA3D and analysis produce very similar amplification function spectra.

CONCLUSIONS

By comparing the results of DYNA3D calculations on the dynamic plastic buckling of imploded OFHC copper cylindrical shells with those from classical analysis and exper-

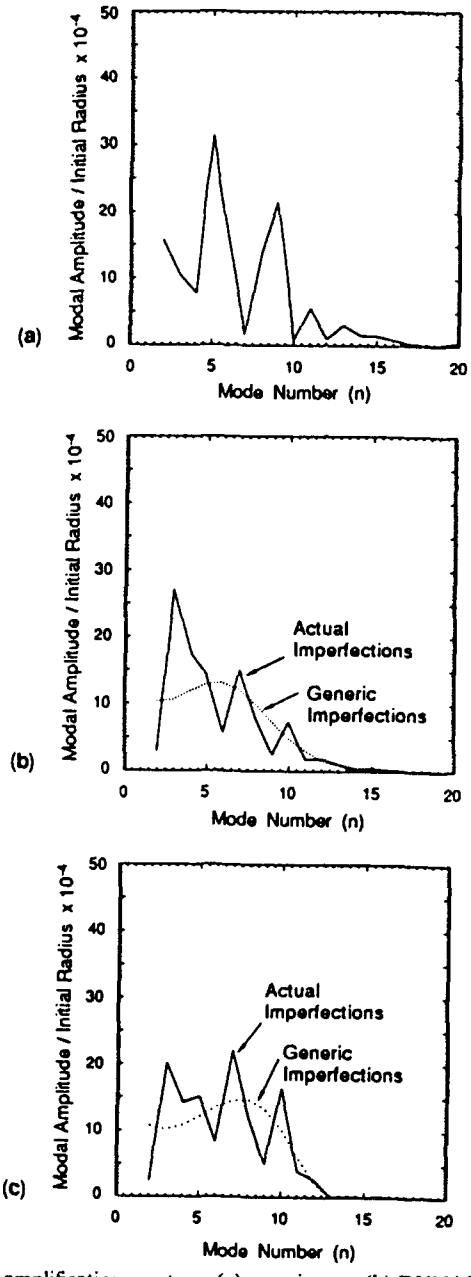

Fig. 10. Modal amplification spectras: (a) experiment; (b) DYNA3D; (c) analysis.

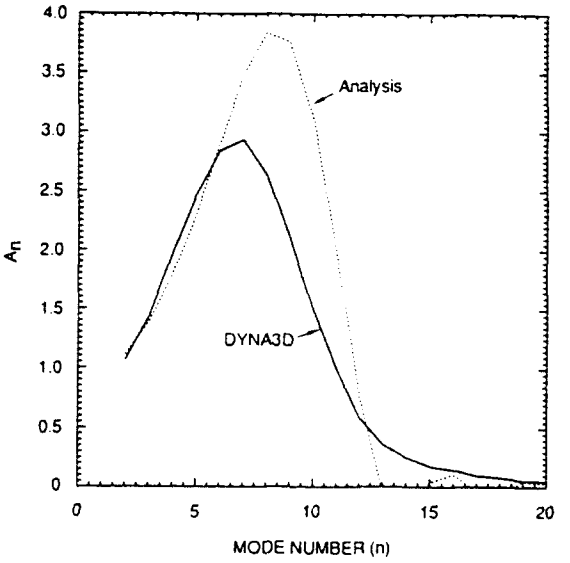

Fig. 11. DYNA3D and analysis amplification function spectra.

Table 1. Comparison of results

	max |w| (mm)	Pref. n	$\max \frac{W_n}{a} \times 10^{-4}$
Experiment	0.26	5–9	32
DYNA3D	0.19	3–8(6)†	27 (13)†
Analysis	0.23	3–10 (7, 8)†	22 (15)†

†With generic imperfections.

imental results a measure of confidence was acquired for application of the code to more complex problems involving dynamic plastic buckling. The agreements of profiles, amplification spectra and amplification functions are good, especially for a description of plastic instability that grows exponentially with time.

Acknowledgements—The authors wish to thank G. R. Cartwright for assistance with the experiments. The work was supported for the most part by the Aerojet Ordnance Company.

REFERENCES

Florence, A. L. (1965). Traveling force on a Timoshenko beam. *J. Appl. Mech. Trans. ASME* **32**, 351–359.
Hallquist, J. O. (1988). DYNA3D users manual. (Nonlinear dynamic analysis of structures of three dimensions.) Lawrence Livermore National Laboratory, report UCID-19592, revision 4.
Johnson, G. R. and Cook, W. H. (1983). A constitutive model and data for metals subjected to large strains, high strain rates, and high temperatures. *Proc. 7th Int. Symp. on Ballistics*, The Hague, The Netherlands.
Kirkpatrick, S. W. and Holmes, B. S. (1989). The effects of initial imperfections on dynamic buckling of shells. *ASCE J. Engng Mech.* **115**(5), 1075–1093.
Lindberg, H. E. and Florence, A. L. (1987). *Dynamic Pulse Buckling*. Martinus Nijhoff, The Netherlands.
Rajendran, A. M. and Bless, S. J. (1985). High strain rate material behavior. Final report under Contract AFWL-TR-85-4009 to Air Force Wright Aeronautical Laboratories.
Romander, C. M. (1987). Sheet explosive simulation for AKM model tests. Final Report under Contract PO8357 to Kaman Sciences Corporation.

APPENDIX

The initial velocity imperfections were obtained from measurements of the explosive thickness. The thickness sampling was taken at 64 equidistant points on a line that becomes circumferential when the explosive is wrapped

around the attenuator. Let $h_e(\theta)$ be the thickness and $\bar{h}_e$ be the average thickness. Then, the departure from the average is $\Delta h_e(\theta) = h_e(\theta) - \bar{h}_e$. The Fourier representation of the thickness variation is

$$\frac{\Delta h_e(\theta)}{\bar{h}_e} = \sum_{1}^{N} \{a_n \cos(n\theta) + b_n \sin(n\theta)\} = \sum_{1}^{N} c_n \cos(n\theta + \phi_n),$$

where the coefficients are evaluated from the data points, α, by

$$a_n = \frac{2}{N} \sum_{\alpha=0}^{N-1} (\Delta h_e/\bar{h}_e)_\alpha \cos(2\pi n\alpha/N)$$

$$b_n = \frac{2}{N} \sum_{\alpha=0}^{N-1} (\Delta h_e/\bar{h}_e)_\alpha \sin(2\pi n\alpha/N)$$

$$c_n = |(a_n^2 + b_n^2)^{1/2}| \quad \phi_n = \tan^{-1}(-b_n/a_n)$$

and $N = 64$. The values of c_n are plotted in Fig. 3.

The final profile was treated similarly except that $N = 2048$. If the dimensionless representation is

$$u(\theta, \bar{\tau}) = \sum_{n=2}^{\infty} |\bar{u}_n| \cos(n\theta + \phi_n),$$

where $u(\theta, \bar{\tau}) = w(\theta, \bar{t})/a_0$, $w(\theta, \bar{t})$ being the final perturbed radial displacement, and we wish to plot $|u_n|$ as in Fig. 9 we note that

$$u(\theta, \bar{\tau}) = \sum_{n=2}^{\infty} \{D(\bar{\tau}) \cos(n\theta) + E(\bar{\tau}) \sin(n\theta)\},$$

where

$$D_n(\bar{\tau}) = \frac{2}{N} \sum_{\alpha=0}^{N-1} u_\alpha \cos(2\pi n\alpha/N) = \bar{D}_n$$

$$E_n(\bar{\tau}) = \frac{2}{N} \sum_{\alpha=0}^{N-1} u_\alpha \sin(2\pi n\alpha/N) = \bar{E}_n.$$

Hence,

$$|\bar{u}_n| = |(\bar{D}_n^2 + \bar{E}_n^2)^{1/2}|.$$

Note that the final amplification function is given by

$$A_n(\bar{\tau}) = |\bar{u}_n|/vc_n.$$